# Supporting Information

## Unassisted Visible Solar Water Splitting with Efficient Photoelectrodes Sensitized by Quantum Dots Synthesized via an Environmentally Friendly Eutectic Solvent-Mediated Approach

Uma V. Ghorpade, ‡[a] Mahesh P. Suryawanshi, ‡[a] Seung Wook Shin,[b] Jihun Kim,[c] Soon Hyung Kang,[d] Jun-Seok Ha,[e] Sanjay S. Kolekar,[a,f]* and Jin Hyeok Kim[a]**

[a.] *Department of Materials Science and Engineering and Optoelectronics Convergence Research Center, Chonnam National University, 300, Yongbong-Dong, Buk-Gu, Gwangju 500-757, South Korea*

[b.] *Department of Physics and Astronomy and Wright Center for Photovoltaic Innovation and Commercialization, University of Toledo, Toledo, Ohio, 43606, USA*

[c.] *School of Electrical Engineering and Computer Science, Gwangju Institute of Science and Technology, 123 Cheomdangwagi-ro, Buk-gu, Gwangju 61005, South Korea*

[d.] *Department of Chemistry Education and Optoelectronics Convergence Research Center, Chonnam National University, 500-757, South Korea*

[e.] *Department of Chemical Engineering, Chonnam National University, Gwangju 61186, Republic of Korea*

[f.] *Analytical Chemistry and Material Science Research Laboratory, Department of Chemistry, Shivaji University, Kolhapur 416-004, India*

‡*U.V. Ghorpade and M. P. Suryawanshi contributed equally to this work.*

Corresponding author: (Jin Hyeok Kim) and (Sanjay S. Kolekar)

Email: jinhyeok@chonnam.ac.kr, ssk_chem@unishivaji.ac.in
TEL: +82-62-530-1709: Fax: + 82-62-530-1699

## Chemicals

All chemicals of analytical grade used throughout the current research includes, Cu (II) acetate (Cu $(CO_2CH_3)_2$, 98%), Sb (III) acetate $(CH_3CO_2)_3Sb$, 99.99%), thioacetamide ($CH_3CSNH_2$, 98%), nickel sulfate ($NiSO_4 \cdot 6H_2O$, 98%), potassium persulfate ($K_2S_2O_8$, 99.99%), hydrochloric acid (HCl, 35~38%), titanium (IV) butoxide (Ti $(OCH_2CH_2CH_2CH_3)_4$, 97%), zinc nitrate (Zn $(NO_3)_2 \cdot 6H_2O$, 98%), sodium sulfide ($Na_2S \cdot 9H_2O$, 99.99%), ethanol ($C_2H_5OH$, 99.99%), ammonia ($NH_4OH$, 28~30%) were purchased and used as received from Sigma Aldrich.

## NiO Seed layer formation

In a typical experiment, fluorine doped tin oxide (FTO) (Pilkington TEC glassTM) used as a transparent conducting glass substrates with sheet resistance of 8-10 $\Omega/cm^2$, were successively cleaned by sonication in acetone, ethanol and distilled water before used for deposition. Thin seed layer of NiO on the FTO substrate is deposited by using precursor solution prepared from nickel acetate, ethanolamine, and ethanol by refluxing followed by spin coating.[1-2] As synthesized film was annealed at 450 $^oC$ in a muffle furnace for 1 h and used further.

## Growth of mesoporous 2D NiO nanosheets using chemical bath deposition (CBD) method

The mesoporous NiO films were deposited on a seeded substrate using a low temperature, simple CBD method. A separate solution of 0.1 M $NiSO_4 \cdot 6H_2O$ and 0.025 M $K_2S_2O_8$ were prepared by dissolving respective compounds in 20 ml of deionized water (DI). Both solutions were mixed in a 50 ml beaker. Further, aqueous ammonia was added dropwise to maintain the exact pH of the precursor solution. Next, seeded FTO substrates were well positioned in the beaker with maintaining 80$^oC$ bath temperature. To obtain the desired thickness, films were taken out at respective time of 2 h and allowed to cool. Afterwards, the resulting film, which was covered with a bit white coating of $Ni(OH)_2$, was washed with water. The perfect mesoporous NiO nanostructures were formed by annealing the samples in air atmosphere at 450 $^oC$ in a muffle furnace for 1 h.

## Growth of 1D $TiO_2$ nanorods using a hydrothermal method

The procedure for the growth of $TiO_2$ nanorods was adopted from our previously published paper.[3] Accordingly, 11.3 ml volume of each DI water and hydrochloric acid (35 ~ 38%) were mixed, followed by the addition of 0.189 mL of titanium (IV) butoxide (97%) after deep stirring forms the precursor solution. The solution was used to deposit $TiO_2$ nanorod films by hydrothermal method by using Teflon-lined stainless steel autoclave at 150 °C for 9 h in a vacuum dry oven. Further, films were annealed in air atmosphere at 450 $^oC$ in a muffle furnace for 30 min.

## Sensitization of CQDs onto $TiO_2$ nanorods and NiO nanosheets

After sintering at respective temperatures, films are allowed to cool and used for the sensitization. Cu-Sb-S based colloidal solution were prepared in toluene following our previously published procedure.[4] CQDs were directly grown on the obtained NiO and $TiO_2$ film by top-down suspending the films in colloidal solution of $Cu_3SbS_4$ and $CuSbS_2$ CQDs respectively. Further, films were rinsed with DI and used as corresponding photoelectrodes.

## Passivation of CQDs sensitized photoelectrodes with a thin ZnS layer using successive ionic layer adsorption and reaction (SILAR) method.

A thin ZnS passivation layer was deposited onto CQDs sensitized photoelectrodes using SILAR method reported in previously published work with slight modifications.[5, 6] More specifically, photoelectrodes were passivated with 6 cycles of ZnS by using commercially available Zn $(NO_3)_2$ as a cationic basis and $Na_2S$ as an anionic basis in distilled water. The adsorption and reaction time for each cycle were 90 s for both $Zn^{+2}$ and $S^{-2}$ sources, and the rinsing time was 20 s at room temperature.

## Characterization

The structural properties of the nanostructures were examined by X-ray diffraction (XRD, PANalytical, X'Pert-PRO Netherlands, voltage: 45 kV, current: 40 mA with Ni-filtered Cu-Kα radiation (λ = 1.54056 Å. Field Emission Scanning Electron Microscopy (FE-SEM, S4800, HITACHI Inc., voltage: 10 kV and current: 20 mA) and High-resolution Transmission electron microscopy (HR-TEM, JEOL-3010, acceleration voltage of 300 kV) was used to study the morphology. The elemental mapping images were analyzed by an energy-dispersive X-ray spectra (EDS) attached to the field emission scanning electron microscope (FE-SEM, Model Hitachi S 4800, Japan) measured at Korean Basic Science Institute, Gwangju. The thickness of thin NiO seed

layer and ZnS passivation layer was measured by LSE strokes Ellipsometer (Model: 7109-C370A, USA). TEM sampling was carried out by drop casting of CQDs dispersed in toluene onto carbon meshed nickel TEM grids (200 meshes, Structure Probe, Inc.). The UV-Visible spectra of each photoelectrode were obtained with Cary 100 (Varian, Mulgrave, Australia) spectrometer at room temperature. Valence band offset (VBO) was measured with ultraviolet photoelectron spectroscopy (UPS) (Thermo VG Scientific, UK) with He I (21.22 eV) radiation source. The chemical states of nanostructures were examined using a high-resolution X-ray photoelectron spectroscopy (HR-XPS, VG Multi lab 2000, Thermo VG Scientific, UK) with a monochromatic Mg-Kα (1253.6 eV) radiation source.

## Photoelectrochemical (PEC) measurements

The PEC measurements were carried out by following our previously used analysis.[3] The PEC measurements of three-electrode and two-electrode configuration were carried under light illumination using a potentiostat (CHI Instruments, USA) with Pt plate as a counter electrodes and saturated (sat.) Ag/AgCl (3.5 M KCl) electrodes as a reference electrode. The linear sweep voltammetry (LSV) measurements of each photoelectrode were carried out in a water splitting setup in three electrode configurations with respective (individual) photoelectrode as working electrode where the photoelectrodes were front side illuminated. During PEC measurement of two-electrode configuration, electrodes kept parallel to each other and illuminated from different side as per the requisite. Samples were used as working electrodes with an active area of 0.2 $cm^2$. Nitrogen bubbled aqueous electrolyte of 0.1 M $Na_2SO_4$ (pH 6.8) was used during PEC measurements. The Ag/AgCl reference electrode was calibrated to the reversible hydrogen electrode (RHE), and thus, the potentials in the 0.1 M $Na_2SO_4$ solution is expressed by the standard Nernst equation. A Xe lamp was used as a light source at 150 W with a light intensity of 100 $mW/cm^2$ with an AM 1.5 filter. Linear sweeps voltammograms (LSVs) under the chopped light on/off illumination were performed at a scan rate of 10 mV/s during the potential sweep. Electrochemical impedance spectroscopy (EIS) was measured in the same electrochemical configuration and electrolyte under the condition of 1 sun of illumination. The frequency ranged from 0.1 Hz to 10 kHz with amplitude of ±10 mV. Chronoamperometry test was conducted at 0 V (vs RHE) under simulated AM 1.5G illumination. An air-tight three-electrode PEC quartz cell reactor with an Ag/AgCl reference electrode, and a Pt wire counter electrode was used for gas chromatography (074-594-P1E Micro GC Fusion, INFICON) measurements with of MEMS-based micro thermal conductivity detector (μTCD and a molecular sieve 5Å column. Photocathodes biased at 0 V (vs. RHE) in an aqueous solution of 0.5 M $H_2SO_4$ (pH ~ 0.5) under AM 1.5G simulated sunlight.

## IPCE measurement and calculation

The IPCE was measured in standard three-electrode configuration in the wavelength range of 300 ~ 900 nm using a specially designed IPCE system for PEC water splitting, which uses a 150 W Xenon lamp as a light source for generating the monochromatic beam. The calibration of IPCE system was performed by using an NREL-certified silicon photodiode. For $TiO_2$-based photoelectrodes, IPCE was measured at applied potential of 1.23 V (vs. RHE), whereas for NiO-based photoelectrodes, IPCE was measured at 0 V (vs. RHE). The IPCE measurements carried out using standard procedure as described in the literature survey by renowned scientist working in the area of solar water splitting.[7] Further IPCE was calculated without using any correction factor during the calculation via following equation,

$$IPCE = \frac{Jsc\left(\frac{mA}{cm^2}\right)1239.8\ (V.nm)}{Photon\ flux\left(\frac{mW}{cm^2}\right)\lambda(nm)}$$

where 1239.8 V. nm represents a multiplication of h (Planck's constant) and c (the speed of light), photon flux is the power intensity in $mW/cm^2$ , and l (nm) is the wavelength at which this illumination power is measured.

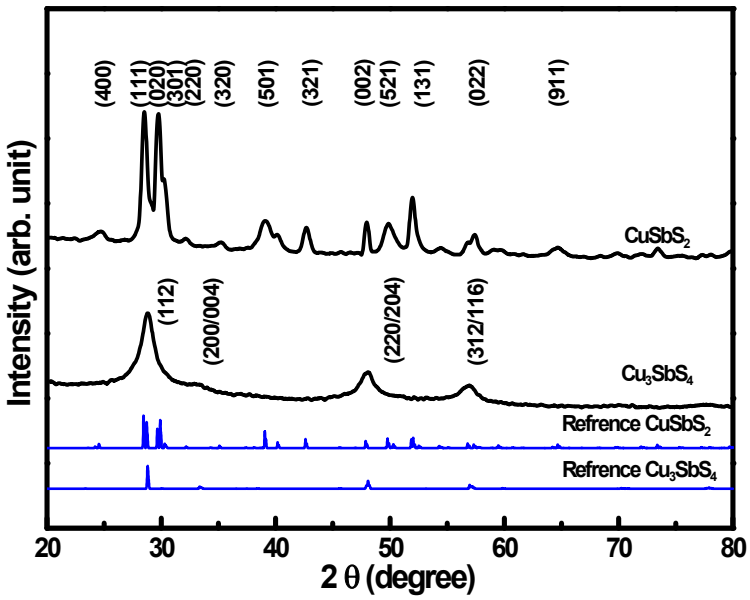


Fig. S1. XRD patterns of $Cu_3SbS_4$ and $CuSbS_2$ CQDs. The reference diffraction patterns are also presented, which exactly matches well with the experimental patterns.

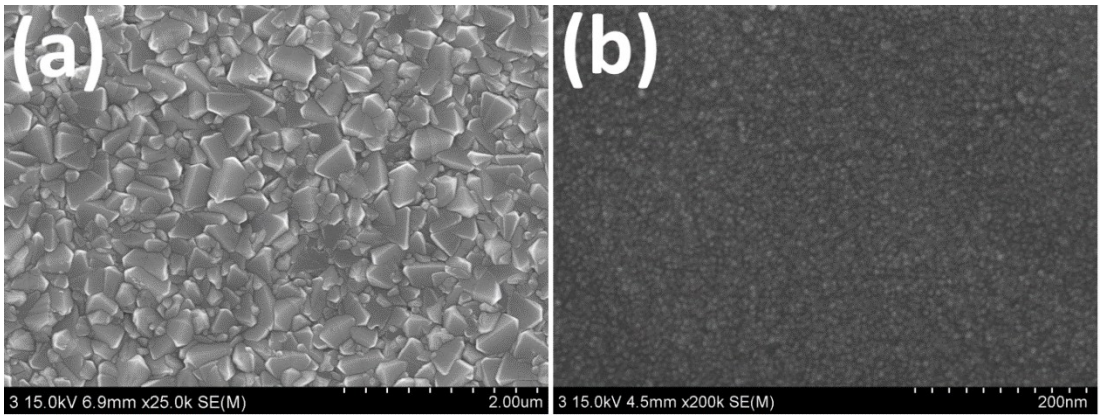


Fig. S2. FE-SEM images of (a) bare FTO and (b) ~ 10 nm of NiO seed layer deposited FTO. NiO seed layer was deposited using spin-coating method before the deposition of NiO nanosheets by chemical bath deposition. Thickness of deposited NiO seed layer was not detectable by FE-SEM image. Corresponding thickness of the film were measured by Ellipsometer.

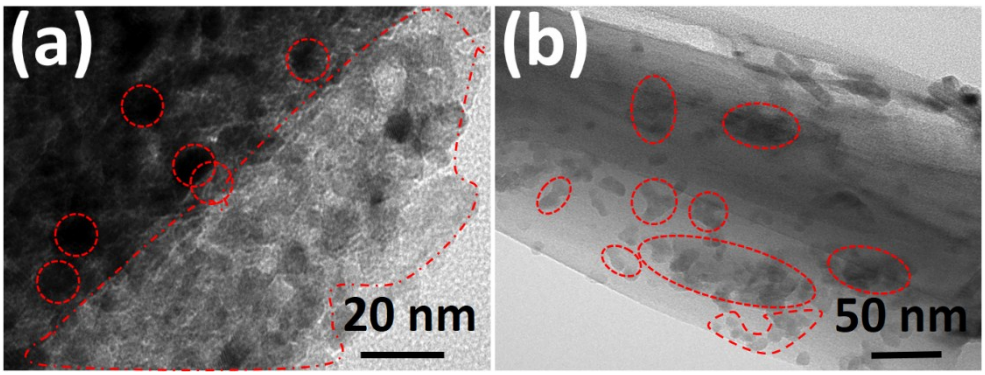


Fig. S3. TEM images of (a) NiO and (b) $TiO_2$ at higher CQDs sensitization time for 10 h. Red circles are CQDs onto NiO and $TiO_2$. Both electrodes show aggregation of CQDs.

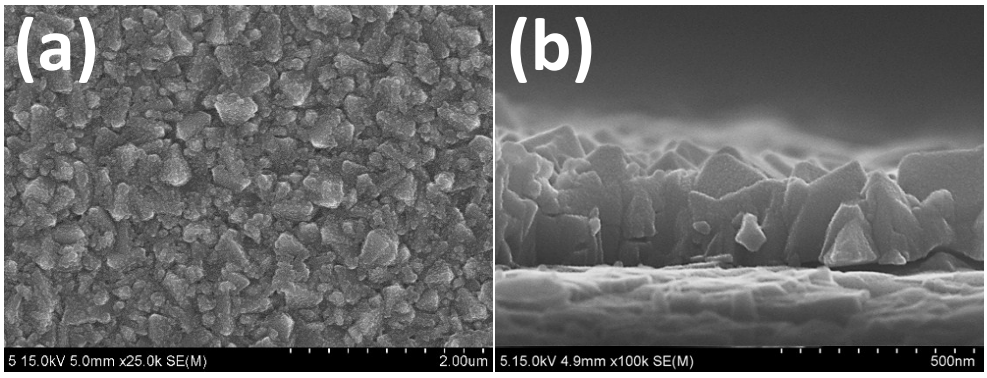


Fig. S4. (a) Surface and (b) cross-sectional FE-SEM images of ZnS passivation layer on FTO grown by SILAR method. Thickness of deposited ZnS layer was not detectable by FE-SEM image, corresponding thickness of ~ 13 nm is measured by Ellipsometer.

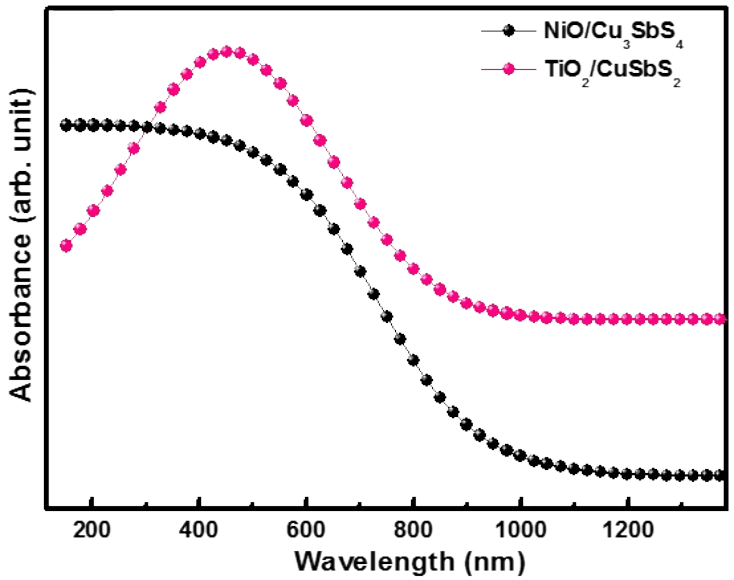


Fig. S5. UV-Vis absorption spectra of $NiO/Cu_3SbS_4$ and $TiO_2/CuSbS_2$ photoelectrodes, respectively.

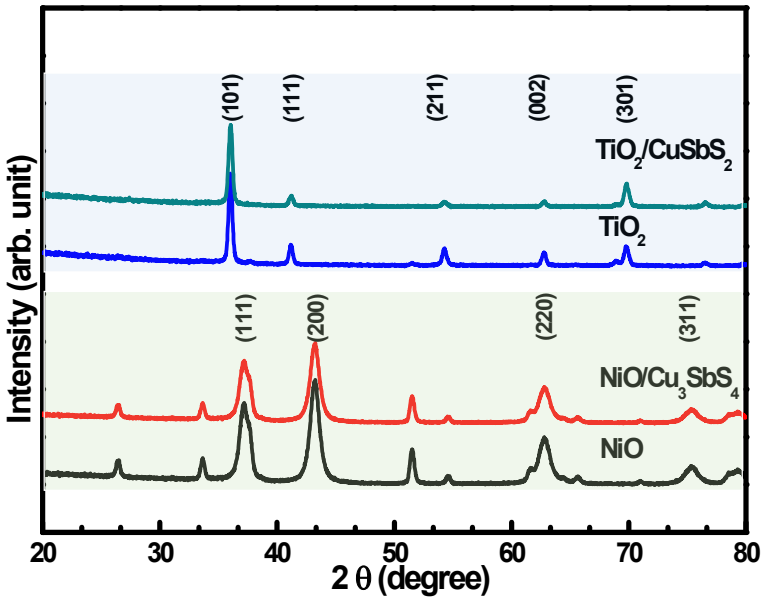


Fig. S6. XRD patterns of bare and sensitized photocathode ($NiO/Cu_3SbS_4$) and photoanode ($TiO_2/CuSbS_2$) materials.

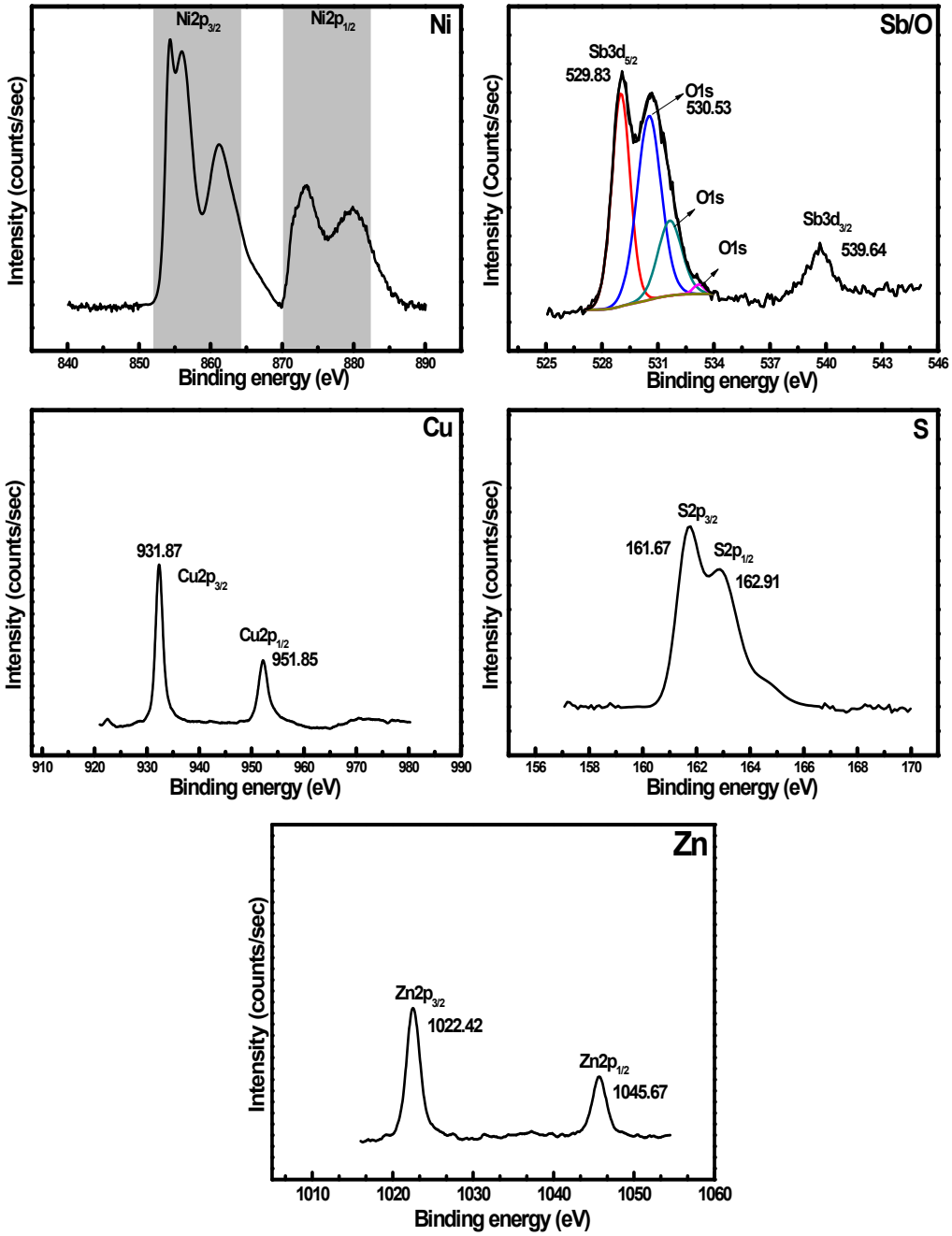


Fig. S7. XPS core level spectra of Ni, Sb, O, Cu, S and Zn elements

from NiO/$Cu_3SbS_4$/ZnS photocathode.

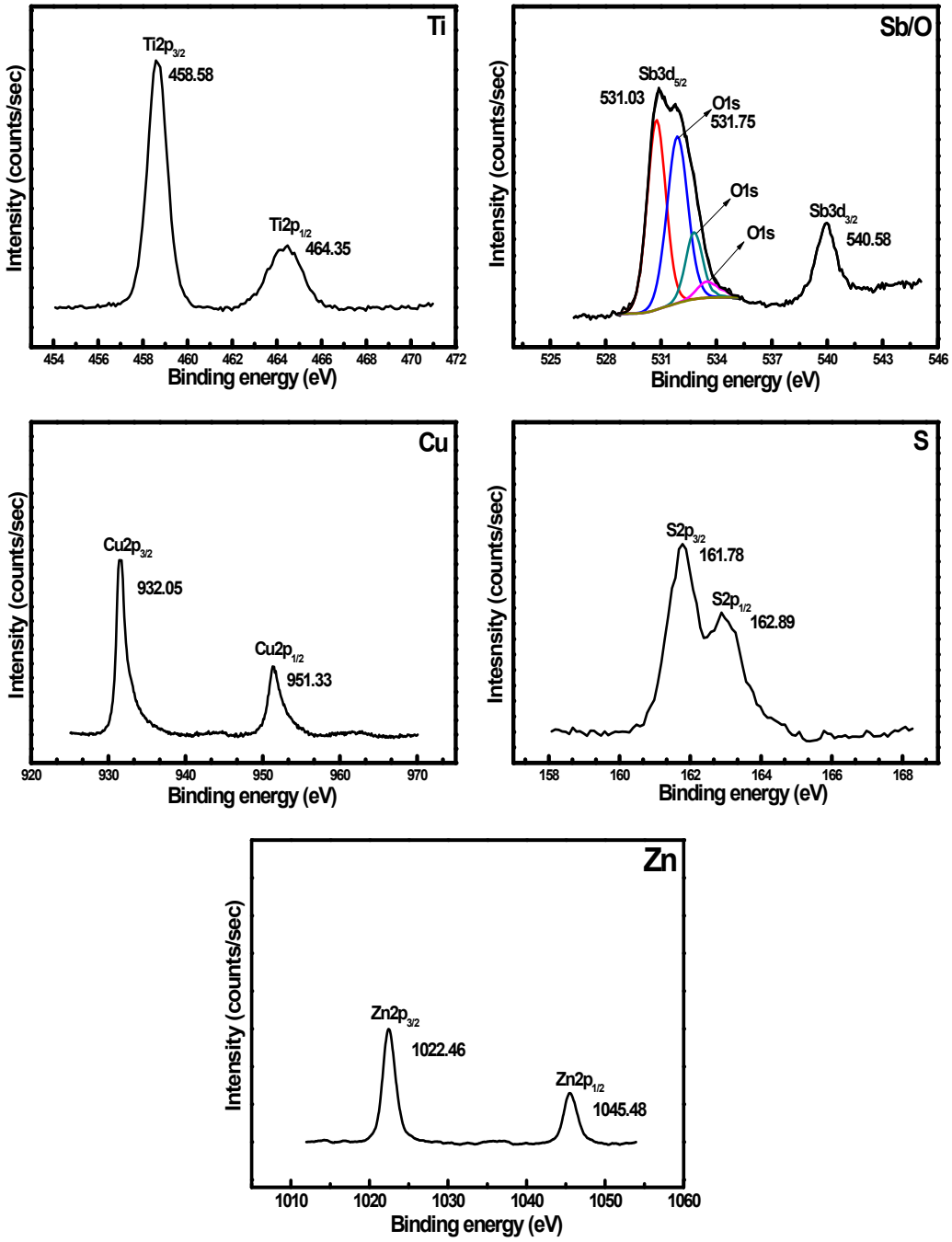

Fig. S8. XPS core level spectra Ti, Sb, O, Cu, S and Zn elements from $TiO_2/CuSbS_2/ZnS$ photoanode.

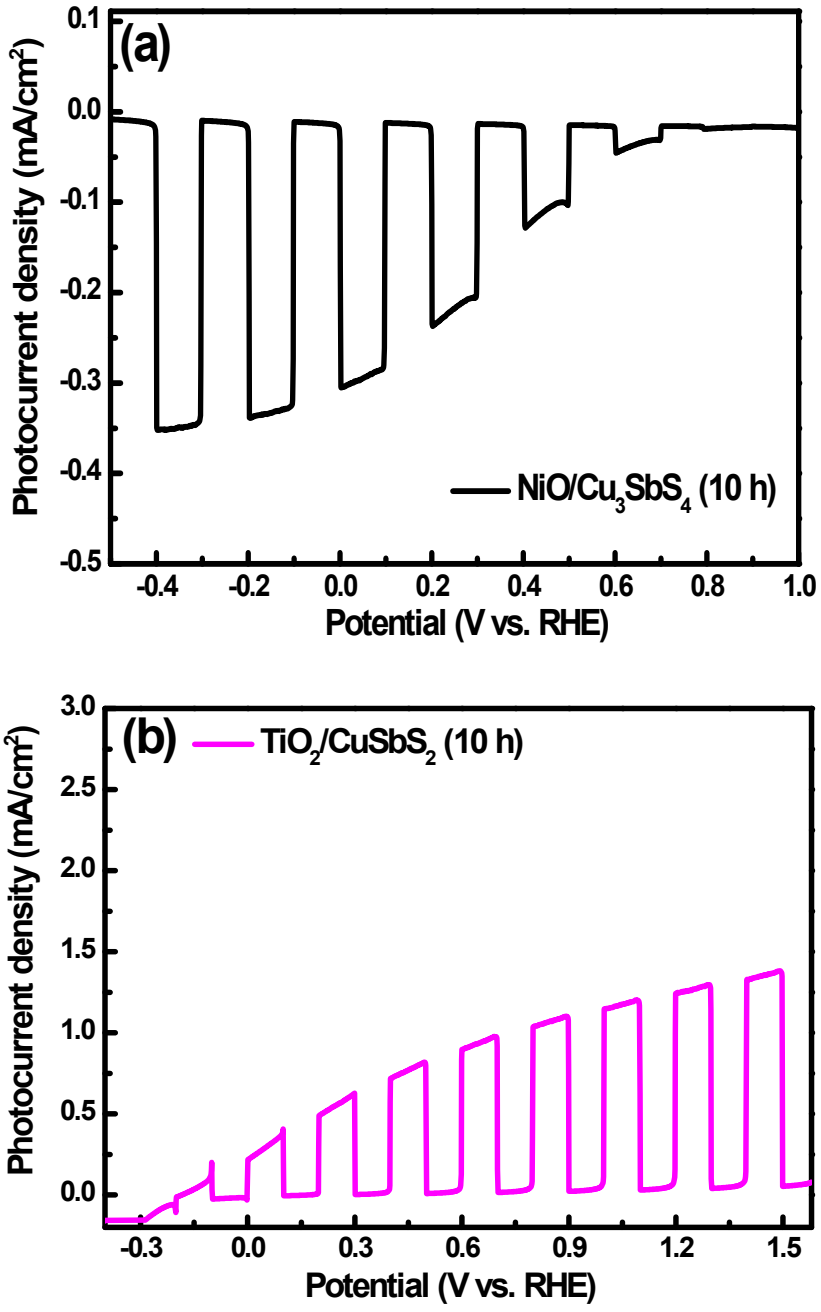

Fig. S9. PEC performance of (a) NiO/$Cu_3SbS_4$ photocathode and (b) $TiO_2$/$CuSbS_2$ photoanode after longer CQDs sensitization time of 10 h. Results showed a decreased photocurrent density at higher sensitization time of 10 h. PEC measurements were carried out with Pt plate as counter electrode and Ag/AgCl as a reference electrode, under 100 $Wm^2$ of Xe lamp and 0.1 M $Na_2SO_4$ electrolyte.

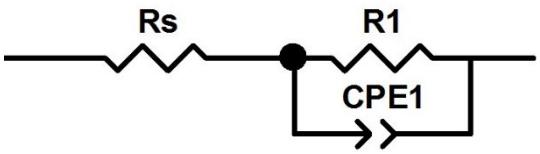


Fig. S10. The equivalent circuit model for bare, sensitized and passivated NiO and $TiO_2$ photoelectrodes. The materials best-fitted to series resistance ($R_s$) and a RC-circuit model.

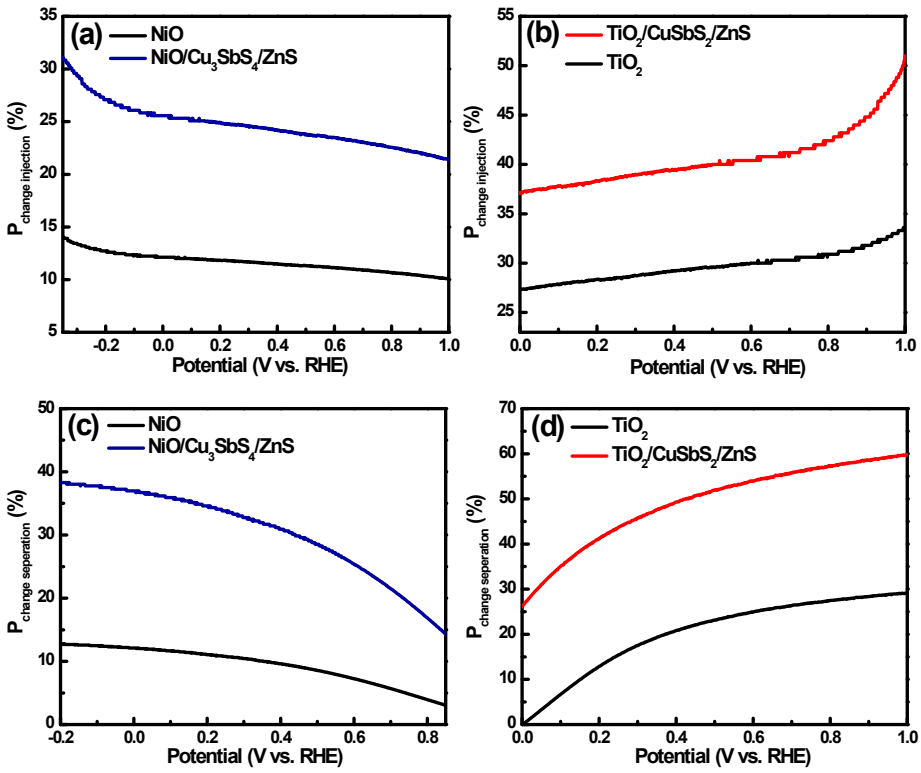


Fig. S11. (a) and (b) charge injection and (c) and (d) charge separation efficiencies of NiO/$Cu_3SbS_4$/ZnS photocathode and $TiO_2$/$CuSbS_2$/ZnS photoanode along with bare NiO and $TiO_2$, respectively.

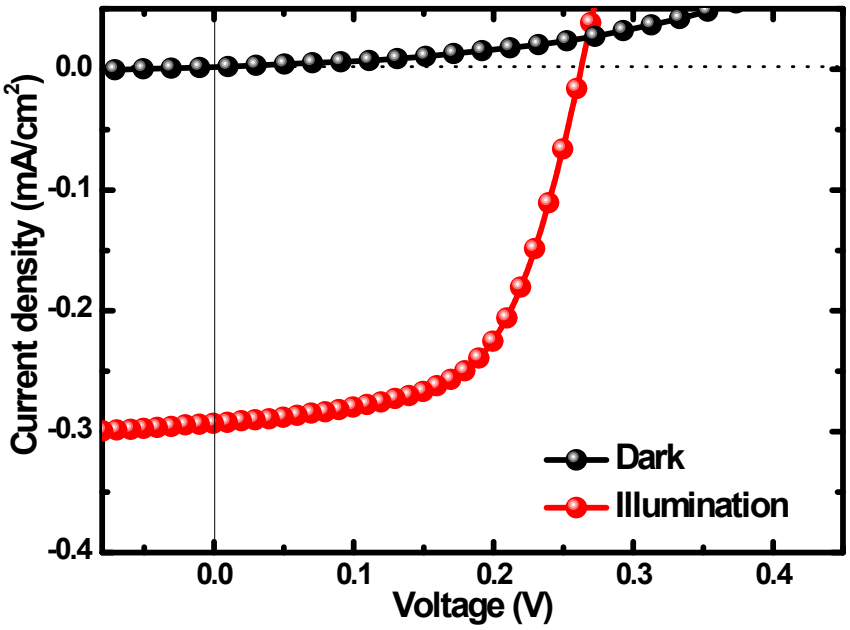


Fig. S12. PEC performance of the tandem electrode system in a two-electrode configuration illuminated from the photocathode side

Fig. S13. Stability measurement of the device system during unassisted water splitting for 50 min. of operation in a two-electrode configuration without ZnS passivation layer.

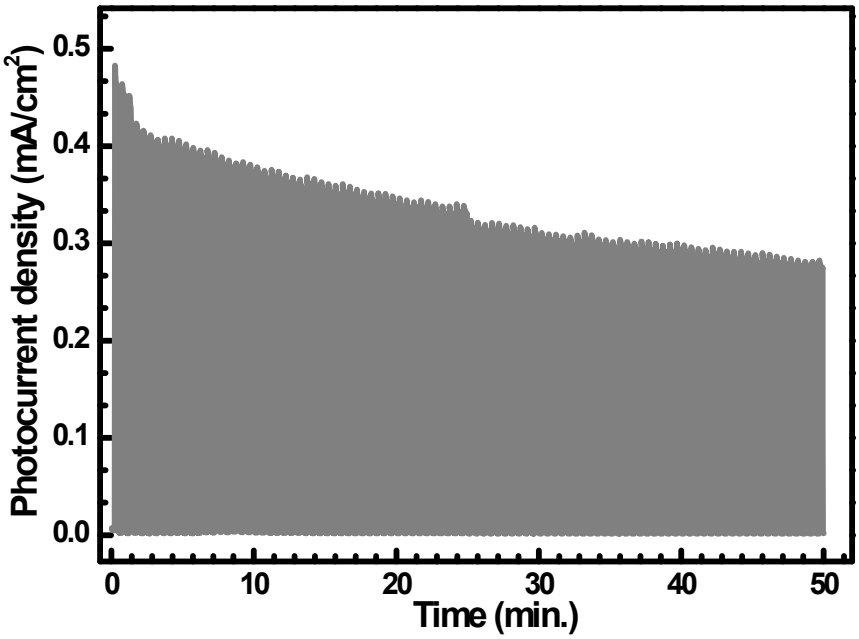


Table S1. Parameters determined from EIS

fitting for bare, sensitized and passivated NiO- and $TiO_2$- based photoelectrodes

| Sample | $R_s$ (Ohm) | $R_{ct}$ (Ohm) | CPE (F) |
|---|---|---|---|
| **NiO** | 136.2 | 1198.7 | $8.681 \times 10^{-5}$ |
| **$NiO/Cu_3SbS_4$** | 130.5 | 912.9 | $3.126 \times 10^{-5}$ |
| **$NiO/Cu_3SbS_4/ZnS$** | 129.6 | 763.3 | $9.231 \times 10^{-4}$ |
| **$TiO_2$** | 36.7 | 939.6 | $3.362 \times 10^{-5}$ |
| **$TiO_2/CuSbS_2$** | 23.2 | 512.4 | $9.152 \times 10^{-4}$ |
| **$TiO_2/CuSbS_2/ZnS$** | 21.9 | 456.1 | $6.451 \times 10^{-4}$ |

CPE: constant phase element

Table S2. Charge injection and charge separation efficiency values for NiO (at 0 $V_{RHE}$) and $TiO_2$ (at 0.8 $V_{RHE}$) based photoelectrodes calculated from Fig. S11.

| Photoelectrode | Charge injection efficiency (%) | Charge separation efficiency (%) |
|---|---|---|
| **Bare NiO** | 12.12 | 12.08 |
| **$NiO/Cu_3SbS_4/ZnS$** | 25.58 | 37 |
| **Bare $TiO_2$** | 30.9 | 27.47 |
| **$TiO_2/CuSbS_2/ZnS$** | 42.40 | 57.16 |

## References:

1. C. J. Flynn, S. M. McCullough, E. Oh, L. Li, C. C. Mercado, B. H. Farnum, W. Li, C. L. Donley, W. You, A. J. Nozik, J. R. McBride, T. J. Meyer, Y. Kanai, J. F. Cahoon, *ACS Appl. Mater. Interfaces,* 2016, **8**, 4754-61.

2. J. R. Manders, S. W. Tsang, M. J. Hartel, T. H. Lai, S. Chen, C. M. Amb, J. R. Reynolds, F. So, *Adv. Funct. Mater.,* 2013, **23**, 2993-3001.

3. M. Suryawanshi, S. W. Shin, U. Ghorpade, D.Song, C. W. Hong, S. S. Han, J.Heo, S. H. Kang, J. H. Kim, *J. Mater. Chem. A,* 2017, **5**, 4695-4709.

4. U. V. Ghorpade, M. P. Suryawanshi, S. W. Shin, I. Kim, S. K. Ahn, J. H. Yun, C. Jeong, S. S. Kolekar, J. H. Kim, *Chem. Mater.* 2016, **28**, 3308-3317.

5. J. Park, M. T. Sajjad, P. H. Jouneau, A. Ruseckas, J. Faure-Vincent, I. D. Samuel, P. Reiss, D. Aldakov, *J. Mater. Chem. A,* 2016, **4**, 827-837.

6. S. Y. Chae, S. J. Park, S. G. Han, H. Jung, C. W. Kim, C. Jeong, O. S. Joo, B. K. Min, Y. J. Hwang, *J. Am. Chem. Soc.* 2016, **138**, 15673-15681.

7. Z. Chen, T. F. Jaramillo, T. G. Deutsch, A. Kleiman-Shwarsctein, A. J. Forman, N. Gaillard, R. Garland, K. Takanabe, C. Heske, M. Sunkara, E. W. McFarland, K. Domen, E. L. Miller, J. A. Turner, H. N. Dinh, *J. Mater. Res.*, 2010, **25**, 3-16.